NURETH-14-500

# Reactor Core Sub-Assembly Simulations Using a Stabilized Finite Element Method

T. M. Smith, J. N. Shadid, R. P. Pawlowski, E. C. Cyr, and P. D. Weber Sandia National Laboratories<sup>1</sup>

## **Abstract**

This paper presents a methodology for solving thermal-hydraulic flows that are prototypical to nuclear reactors, using a stabilized finite element method. The discrete equations are solved using a fully-coupled algebraic multigrid preconditioned Newton-Krylov iterative solver. The prototype problem of interest is a spatially evolving flow through a 3x3 rod bundle geometry including spacer grid and mixing vanes, which is modeled using large eddy simulation at different spatial resolutions. The results demonstrate trends towards convergence of mean values in the far field (as mesh resolution increases), though, the flow field just downstream of the mixing vanes will require greater resolution to capture, than is presented here.

#### Introduction

The Consortium for Advanced Simulation of Light Water Reactors (CASL) is the name of a new U.S. Department of Energy Innovation Hub that is investing in the development of a "virtual reactor toolkit" that incorporates science-base models, state-of-the-art numerical methods, modern computational science, modern software engineering, and uncertainty quantification and validation against currently operating pressurized water reactors. Under CASL there are five focus areas having different responsibilities. One of these, Thermal Hydraulics Methods (THM) is tasked with developing computational fluid dynamics (CFD), multi-phase computational fluid dynamics (MCFD) and thermal-hydraulics (TH) tools that can solve challenge problem flows.

One such challenge problem deals with grid-to-rod-fretting (GTRF). This problem is characterized by flow induced rod vibrations that cause deterioration of the rod cladding material and support grids at points of contact. The vibrations are due to turbulent flow generated at the core inlet and by rod bundle support grid mixing vanes. Turbulence is deliberately generated to enhance heat transfer and prevent localized hot spots from occurring. This problem is inherently three-dimensional and unsteady. High fidelity turbulence modeling will lead to better understanding of rod excitation phenomena and has the potential to improve clad time-to-failure, enhance heat transfer and improve overall reactor core performance.

<sup>&</sup>lt;sup>1</sup> Sandia National Laboratories is a multiprogram science and engineering facility operated by Sandia Corporation, a Lockheed-Martin company, for the U.S. Department of Energy's National Nuclear Security Administration, under contract DE-AC04-94AL850.

Ultimately, full-scale simulations of the entire reactor core including inlet/outlet characterization will be performed. Included in these will be coupled fluid/structure interaction simulations. Leading up to full-scale, various sub-scale rod bundle assembly problems serving as prototypes will be solved and analyzed. Separate fluid and structural dynamic simulations will be conducted where the rod excitation predicted by the fluid simulations will be transferred to the structural code through surface boundary conditions.

Our initial prototype problem is turbulent flow through a 3x3 rod bundle with support grid and mixing vanes. A new CFD code called Drekar is under development to address the challenge problems. Drekar uses a stream-line upwind Petrov Galerkin (SUPG) stabilized finite element (FE) discretization and solves the equations in a fully coupled manner using a Newton-Krylov nonlinear solver and GMRES iterative linear solver. Time integration is based on a BDF method. Large-eddy simulation (LES) turbulence model methodology has been employed. The wall adapted large eddy (WALE) model developed by Nicoud and Ducros [1] has been used. In two related studies, [2,3] the CD-Adaptco STAR-CCM++ CFD solver [4] and WALE LES sub-grid turbulence model was used to solve for the turbulent flow and rod vibration forcing on the same geometry. This work also follows closely the work by Benhamadouche et al. [5] who used an unstructured finite-volume discretization and SIMPLEC iteration procedure to solve the flow equations to study rod excitation. They used the Smagorinsky sub-grid model along with a wall model for their turbulence model. In another related work, Abbasian et al. [6] used a dynamic Smagorinsky sub-grid model (DSM) in the study of turbulent flow along a circular array of rods. The model was assumed periodic in the streamwise direction so that fully develop turbulent flow could be realized. The DSM alleviates the requirements of specifying a model constant and a wall-damping model. The present work is considered in line with these two studies with the main difference being the numerical methods used in the flow solver.

In this paper LES solutions at four different mesh resolutions will be presented. The next section presents the governing equations, LES turbulence model and discretization details. Next, a description of the problem details is presented. Results from the flow solutions will then be presented followed by a discussion of the results.

## 1. Governing equations

This section presents the governing equations describing; unsteady, single-phase, incompressible isothermal flows.

## 1.1 Flow equations

A summary of the governing equations is presented in Table 1. The equations are written in residual form, which simplifies presentation of the weak form of the FE method.

Governing Equation	
Continuity	$R_{\rho} = \frac{\partial \overline{\rho}}{\partial t} + \overline{\rho} \nabla \circ \overline{\mathbf{u}}$
Momentum	$R_{m} = \frac{\partial \left(\overline{\rho} \overline{\mathbf{u}}\right)}{\partial t} + \nabla \cdot \left(\overline{\rho} \overline{\mathbf{u}} \otimes \overline{\mathbf{u}}\right) - \nabla \cdot \mathbf{T}$

Table 1. Residual form of governing equations for incompressible, isothermal, single-phase flow.

In these equations,  $\overline{\rho}$  is the density,  $\overline{\bf u}$  is the velocity vector, and  ${\bf T}$  represents the stress tensor (containing pressure,  $\overline{P}$ )  ${\bf T} = -\overline{P}{\bf I} + \mu_{\rm eff} \left[ \nabla \overline{\bf u} + \nabla \overline{\bf u}^T \right]$ . The subscript "eff" on viscosity signifies that this coefficient contains both molecular and eddy viscosities,  $\mu_{\rm eff} = \mu + \mu_{\rm r}$ . The eddy viscosity models unresolved turbulent fluctuations. The over bar denotes spatial filtering in LES. The filter operator is mass weighted (Favre) if density is not constant. Boundary and initial conditions are required to complete the mathematical description of the flow problem. The specific boundary and initial conditions are discussed in a later section.

## 1.2 <u>Turbulence modeling</u>

The Reynolds number for this class of flows can typically reach tens to hundreds of thousands and sub-assembly hardware can be several meters in length rendering direct numerical simulation un-tractable. It is therefore necessary to apply averaging or filtering to the governing equations resulting in RANS, URANS or LES models for solving these flows. RANS equations model all of the turbulent fluctuations thus lumping all the physical processes associated with unsteady turbulent fluctuations into effective constitutive parameters such as eddy viscosity or conductivity. Higher fidelity flow analysis has been pursued based on large eddy simulation where two assumptions are made; 1) most of the turbulent transport is carried out by the large scales which are directly computed and 2) the small (sub-grid) unresolved scales are more universal than the large scales and can be described by relatively simple eddy-viscosity models.

Consider a single constituent incompressible fluid. The sub-grid stress tensor arising in the filtered momentum equation is;

$$\tau_{ij}^{sgs} = \overline{\rho} \left( \overline{u_i u_j} - \overline{u_i} \overline{u_j} \right)$$

The sub-grid stress tensor is modeled using the Boussinesq assumption;

$$\tau_{ij}^{sgs} = -2\overline{\rho}v_{i}\overline{S}_{ij} + \frac{1}{3}\tau_{kk}^{sgs}\delta_{ij}$$
$$\overline{S}_{ij} = \frac{1}{2}\left(\frac{\partial\overline{u}_{i}}{\partial x_{j}} + \frac{\partial\overline{u}_{j}}{\partial x_{i}}\right)$$

where  $\overline{S}_{jj}$  is the filtered strain rate tensor. The trace of the sub-grid stress tensor is absorbed

in the pressure;  $\overline{P} = \overline{p} - \frac{1}{3} \tau_{kk}^{sgs} \delta_{ij}$ , and recognizing that  $\mu_i = \overline{\rho} v_i$ , results in the LES equations presented in Table 1.

The eddy viscosity is typically evaluated using a variation of the Smagorinsky model [7] that accounts for the presence of solid surfaces. An example is Van Driest damping which is suitable for wall-bounded flows [8,9];

$$v_{i} = \left(C_{S}\Delta\left[1 - \exp\left(-y^{+}/A^{+}\right)\right]\right)^{2} \left|\overline{S}_{ij}\right|$$

where  $C_s$  is a model constant,  $\Delta = \Omega_e^{1/3}$ , is the cube root of the element volume,  $|\overline{S_y}| = \sqrt{2\overline{S_y}\overline{S_y}}$ ,  $A^+ = 26$ ,  $y^+ = yu_\tau/v$ ,  $u_\tau = \sqrt{\tau_w/\overline{\rho}}$  and  $\tau_w$  is the wall shear stress. Note  $y^+$  may not be a local quantity depending on its interpretation and code implementation. The model used in this study is called wall adapting local eddy-viscosity (WALE). The WALE model introduced by Nicoud and Ducros [1] is an modified Smagorinsky eddy viscosity model where the filter width is based on the square of the deviatoric stress tensor and requires only "local data" to construct. In addition to being a "local" model, it recovers the proper  $y^3$  near-wall scaling for the eddy viscosity so eddy that it inherently decays to zero as the wall is approached without using a dynamic procedure or wall model. The eddy-viscosity model is defined as;

$$\upsilon_{t} = \left(C_{w}\Delta\right)^{2} \frac{\left(\overline{S}_{ij}^{cl} \overline{S}_{ij}^{cl}\right)^{3/2}}{\left(\overline{S}_{ij}^{cl} \overline{S}_{ij}^{cl}\right)^{5/2} + \left(\overline{S}_{ij}^{cl} \overline{S}_{ij}^{cl}\right)^{5/4}}$$

$$\overline{S}_{ij}^{cl} = \overline{S}_{ik} \overline{S}_{kj} + \overline{\Omega}_{ik} \overline{\Omega}_{kj} - \frac{1}{3} \delta_{ij} \left[\overline{S}_{mn} \overline{S}_{mn} + \overline{\Omega}_{mn} \overline{\Omega}_{mn}\right]$$

$$\overline{\Omega}_{ij} = \frac{1}{2} \left(\frac{\partial \overline{u}_{i}}{\partial x_{j}} - \frac{\partial \overline{u}_{j}}{\partial x_{i}}\right)$$

where  $\overline{S}_{ii}^{d}$  is the square of the deviatoric stress tensor,  $\overline{\Omega}_{ij}$  is the rotation tensor and  $C_{iv} = 0.55$ 

## 2. Spatial and temporal discretization

The code is designed to solve the low-flow Mach number Navier-Stokes system. In this section we very briefly describe the stabilized FE methods used for discretization of the Navier-Stokes equations for incompressible and isothermal transient flow. The governing PDEs for the flow are presented in Table 1.

## 2.1 Stabilized FE discretization

The stabilized FE formulation in Table 2 [10,11] allows the use of equal order interpolation for both velocity and pressure and removes spurious pressure oscillations from the null space of the

operator and also implements a streamline-upwind capability to limit oscillations that can be generated due to unresolved gradients in high grid Reynolds number flows. The stabilized FE formulation has been shown numerically to be 2<sup>nd</sup> order accurate in space and time on smooth solutions when combined with an appropriate semi-discrete time discretization (e.g. Trapezoidal rule, BDF2, or Midpoint rule).

Governing Equation	Stabilized FE Weak Form Residual Equation for Low Mach Number Flow
Momentum	$F_{m,i} = \int_{\Omega} \Phi R_{m,i} d\Omega + \sum_{e} \int_{\Omega_{e}} \tau_{m}(\overline{\mathbf{u}} \cdot \nabla \Phi) R_{m,i} d\Omega$
Continuity	$F_{p} = \int_{\Omega} \Phi R_{p} d\Omega + \sum_{e} \int_{\Omega_{e}} \overline{\rho} \tau_{m} \nabla \Phi \cdot \mathbf{R}_{m} d\Omega$

Table 2. Stabilized FE weak form residuals for the governing PDEs. The first term is the Galerkin term, followed by the SUPG term.

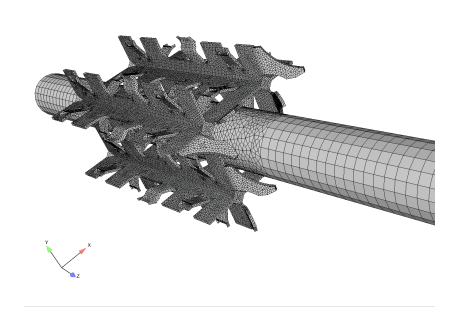
# 2.2 <u>Preconditioned Newton-Krylov method</u>

The result of a fully-implicit solution technique is the construction of very large, coupled highly nonlinear algebraic system(s) that must be solved. Therefore, these techniques place a heavy burden on both the nonlinear and linear solvers and require robust, scalable, and efficient nonlinear solution methods. In the present code, Newton-based iterative nonlinear solvers [12] are employed to solve the nonlinear systems that result in this application. These solvers can exhibit quadratic convergence rates independently of the problem size when sufficiently robust linear solvers are available. For the latter, we employ Krylov iterative techniques. A Newton-Krylov (NK) method [13,14] is an implementation of Newton's method in which a Krylov iterative solution technique is used to approximately solve the linear systems,  $\mathbf{J}_{k}\mathbf{s}_{k+1} = -\mathbf{F}_{k}$ , that are generated at each step of Newton's method. The Jacobian matrix,  $\mathbf{J}_{k}$ , that is used for the Jacobian-vector products in the Krylov solvers, and as the basis for computing the preconditioners described here, is developed from automatic differentiation (AD) techniques.

For the considered class of linear systems described above, convergence is only achieved with preconditioning due to ill-conditioning in the underlying matrix equations [15]. Traditionally, Schwarz domain decomposition (DD) with block incomplete factorization, ILU(k) has been used to precondition the systems. However, these techniques do not scale well as the problem size is increased. In fact, the number of iterations required, to solve the linear system, increases as the number of processors is increased. Instead, algebraic multi-grid (AMG) solution methods will be used [16]. The advantage of AMG is that coarsened representations of the operators are used to effectively transfer information across the global domain and increase the convergence rate of the fine mesh iterative solvers. Using these techniques, the growth in the iteration count can be limited as the number of unknowns, and also as the number of processors is increased. In many cases these methods can lead to optimally converging iterative methods where the number of iterations to solution is independent of problem size and processor count [17,18].

# 3. Description of the problem

This section describes the computational domain, grids, flow conditions and boundary conditions used to define the flow problem in an idealized sub-assembly reactor core fuel rod bundle model. A portion of the geometry is presented in Figure 1 and a summary of flow conditions and boundary conditions are listed in Table 3. The image on the left of Figure 1 shows the center rod surface and the surrounding support grid spacers and mixing vanes. The domain spans 17.86 rod diameters with 3.11 diameters upstream of the spacer and 10.74 diameters downstream of the spacer. The original geometry was 54.94 diameters, however, was shortened to reduce the mesh sizes and computational cost. Exploratory simulations were conducted demonstrating that the mean pressure decays nearly to zero ten diameters downstream of the mixing vanes [18]. The right side of Figure 1 shows a top view of the grid spacer with mixing vanes and the proximity of the inner and outer rods. The location and orientation of the periodic boundaries are also labeled.



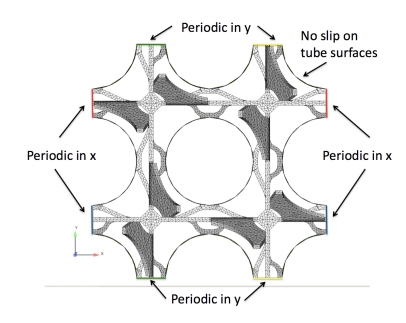


Figure 1. Images of problem geometry. Left image is the coarse 672K CUBIT HEX element mesh with mixing vane and center tube. Right image is a schematic of the (x,y) plane boundary conditions.

Quantity	Description	Value
Inlet boundary condition (z-plane)	Specified constant velocity	$\mathbf{v} = (0, 0, 5  m/s)$
Outlet boundary condition (z-plane)	Zero stress	$T \circ n = 0$
Rod surface (x,y)	No-slip	$\mathbf{v} = 0$
Inner-sub-channel flow surfaces	Periodic	
(x,y)		
H <sub>2</sub> 0 Fluid Properties	Temperature	394.2K
H <sub>2</sub> 0 Fluid Properties	Viscosity	2.32x10 <sup>-4</sup> Pa sec
H <sub>2</sub> 0 Fluid Properties	Density	$942.0 \text{ kg/m}^3$

Table 3. Description of boundary conditions and fluid properties.

The computational grids were generated using Sandia National Laboratories CUBIT [19] mesh generating software. The geometry was supplied by Westinghouse Electric Corporation (WEC) [2,3] in the form of a CAD file. The meshing strategy consisted of first generating a mesh comprising tetrahedral elements and then sub-dividing each tetrahedral into hexahedral elements. A smoothing algorithm was then applied to each mesh to improve element quality.









Figure 2. Cut-planes (z) of the meshes at probe location A (see Table 6).

Examples of the cut-planes of the different mesh resolutions as shown in Figure 2. The problem domain and boundary conditions are designed to model a subset of a rod bundle "ideally" far away from the reactor core walls such that significant cross-flow in the x-y directions can exist.

At the inflow plane, a uniform velocity is assumed and at the outlet, a stress free condition is imposed. All other external flow surfaces are periodic and all solid surfaces are no-slip. The Reynolds number based on rod diameter and mean inlet velocity was 192,800. A summary of flow conditions is shown on Table 3.

## 4. Results

We now present results for the unsteady turbulent flow field for the WEC 3x3 rod assembly [2,3] problem including the grid spacer, for four different mesh resolutions. For the results that follow, BDF2, linear equal-order interpolation, SUPG convection stabilization and the WALE LES subgrid model are used. The results for this study were obtained on parallel machines running from 256 to 1024 cores of the SNL Redsky parallel capacity machine. In preparation for this study Drekar was also ported and run on up to 9600 cores of the ORNL Jaguar platform. The mesh sizes vary from 0.67M to 6M elements (see Table 4).

Mesh	# of	Simulated	Flow	Δt	CFL ave.	Y+ ave.
	elements	time (sec.)	through		(section1/section3)	
			times			
672K	671,572	0.88	26	$5.0 \times 10^{-5}$	9.6/1.3	26
1M	1,049,228	1.11	33	$5.0 \times 10^{-5}$	11.1/2.9	19
3M	2,663,920	0.20	6	$2.0x10^{-5}$	5.9/2.1	16
6M	5,832,718	0.32	9	$2.0x10^{-5}$	7.9/2.2	13

Table 4. Description of computational details for the different mesh resolutions.

The LES simulations were initiated by restarting from Navier-Stokes solutions using only the kinematic viscosity. Therefore, the initial transients have been greatly minimized. In the context

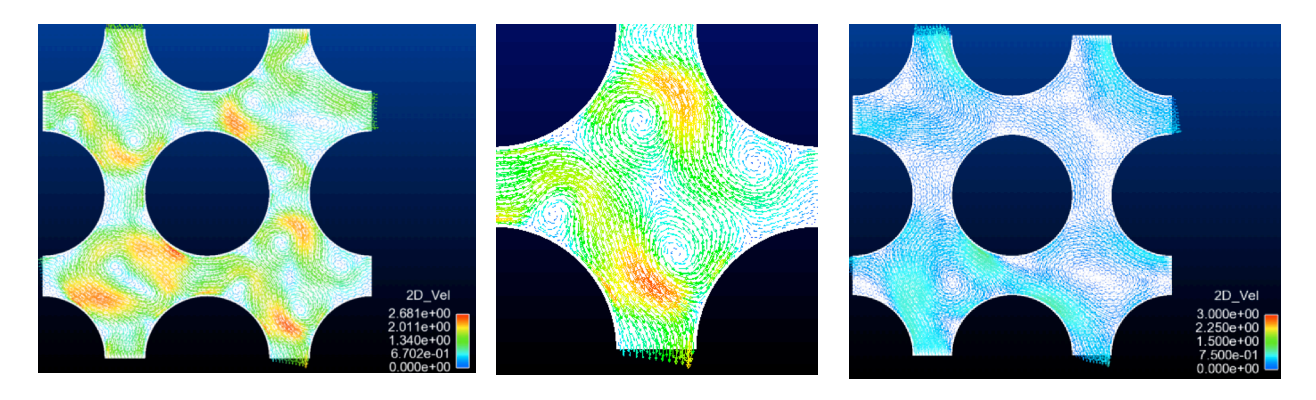


Figure 3. Cut-plane plot of cross-stream velocity. Vectors are colored by cross-stream time-averaged velocity magnitude. Left image is at location A (see Table 6). The middle image is of the lower-right quadrant of the sub-channel cut-plane image and can be compared qualitatively to the Figure 5a and 5b in the WEC simulation of Elmahdi *et al.*, [2]. Right image is at location E.

of the time averaged resolved LES solution data, Figure 3 presents the cross-stream velocity field on a cut-plane located at two locations downstream of the mixing vane strap trailing edge. On the left image (z = 1.8D) recirculation patterns are clearly evident in the sub-channels and indicate the persistence of the swirl generated by the mixing vanes upstream. The detailed image in the middle is of the lower-right sub-channel and can be compared qualitatively to Figures 5a and 5b in the WEC paper of Elmahdi *et al.*, [2] and shows reasonable qualitative agreement with their simulations. The image on the right is from z = 10.53D. At this location, cross-flow is observed.

The average pressure drop across the spacer grid, for four different grid resolutions, is shown in Figure 4. The lines were extracted from the time averaged pressure fields. Clearly, the spacer grid is responsible for most of the pressure drop. The average pressure drop across the grid spacer computed for different mesh resolutions is presented in Table 5. These values were extracted from a single grid point upstream and downstream of the mixer grid.

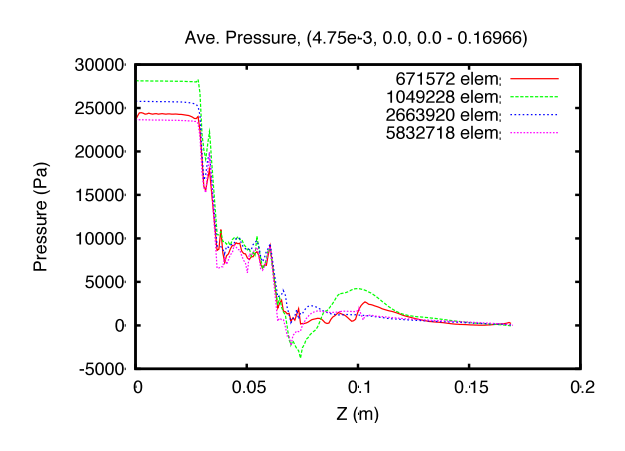
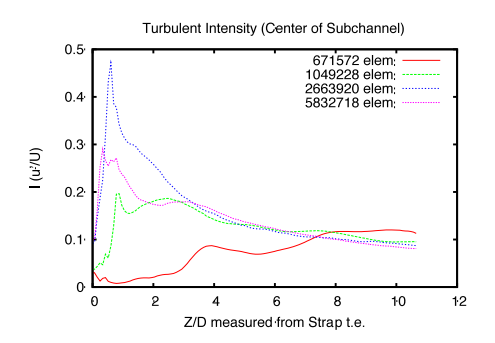


Figure 4. Time-averaged pressure profiles across spacer grid for different grid resolutions.

Mesh	Mean
	Pressure
	Drop (Pa)
667K	23,400
1M	26,780
3M	23,800
6M	22,042

Table 5. Overall time-averaged pressure drop across mixing vane as a function of mesh resolution.

The time averaged turbulence intensity and eddy viscosity along the center of a sub-channel downstream from the strap trailing edge for various mesh resolutions is plotted in Figure 5. The intensity plot shows non-monotonic behavior between the different solutions near the trailing edge, and then converging further downstream. The eddy viscosity plot correctly demonstrates that as the mesh becomes finer, less and less eddy viscosity is produced.



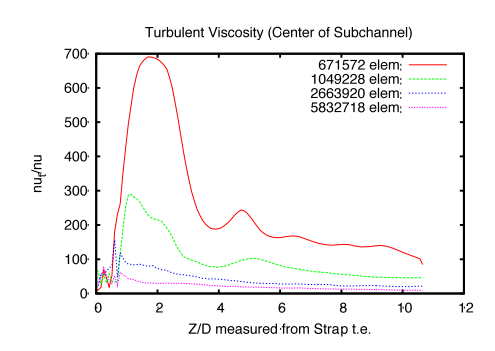


Figure 5. Average turbulence intensity and eddy viscosity along a line in the center of a sub-channel starting at the strap trailing edge.

The time history of the pressure at five locations on the center rod surface for different mesh resolutions is presented in Figure 6. The locations of the probes relative to the spacer grid strap trailing edge are listed in Table 6. Several spikes appearing in the trace data are due to a restart issue. Apart from the coarsest resolution case 672K, the three finer resolution cases show convergence of the average pressure at roughly 5 diameters downstream of the mixer strap trailing edge.

	Probe location relative to	Probe location relative
Probe	strap t.e. (0.00475,0.0,z) m	to strap t.e. normalized
		by rod diameter
Α	0.017	1.80
В	0.030	3.18
С	0.050	5.26
D	0.074	7.78
Е	0.100	10.53

Table 6. Trace probe location relative to spacer grid strap trailing edge.

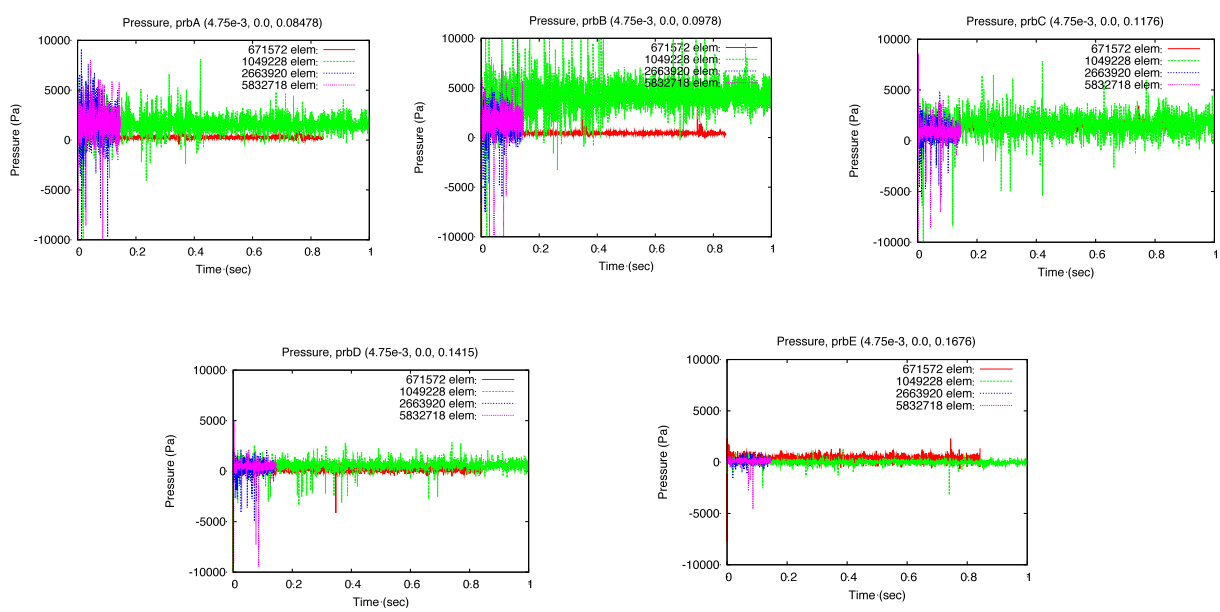


Figure 6. Point-wise data for pressure time history at various locations downstream of the mixing vane.

The fast Fourier transform (FFT) and power spectral density (PSD) of the pressure on the surface of the center rod for the 6M mesh resolution case at probe location A are shown in Figure 7. The maximum frequency of the FFT is roughly the Nyquist frequency. While still only preliminary at this time, the characteristic turbulent cascade is evident in the PSD.

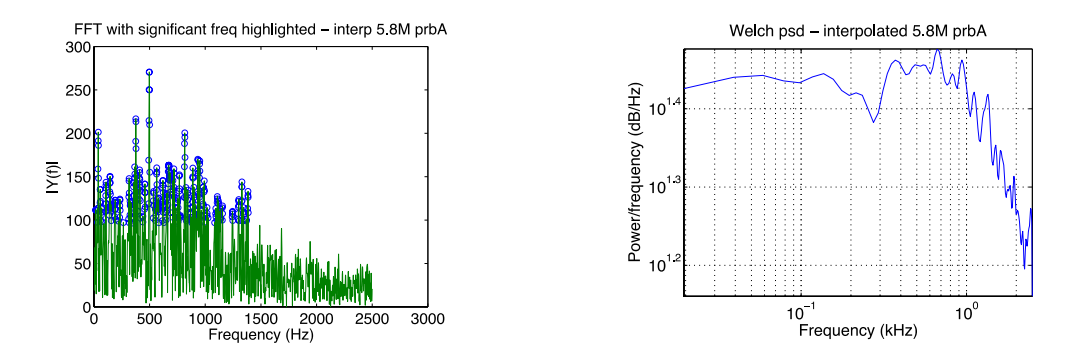


Figure 7. Initial time series analysis of transient pressure signal on center tube of the 3x3 rod assembly. Left image is the FFT and right image is the PSD.

## 5. Discussion

In this work, a stabilized finite element method has been used compute the flow field in a 3x3 rod bundle including the spacer grid and mixing vanes. Solutions on four mesh resolutions have been presented. From Table 3 summarizing the computational details, Figure 2 showing a cutplane of the mesh and Figure 4 showing the pressure drop across the spacer grid, it is clear that the 672K mesh is inadequate to resolve the behavior of pressure for this geometry. On the other

hand, the other three solutions start to show signs of convergence in the mean for pressure drop, upstream of the spacer grid and also approximately six diameters downstream of the strap trailing edge. The mean pressure appears to be less sensitive to spatial and temporal resolution than the velocity field. Considering the average CFL at which time was advanced and the y which gives and indication of how well the boundary layers were resolved, these solutions are not well resolved LES. The lack of spatial resolution is probably responsible for the over prediction of turbulence intensity (~18% at three diameters compared with ~11% predicted by Benhamadouche et al. [5]) and non-monotonic behavior just downstream of the strap trailing edge. However, at three diameters downstream, the turbulence intensity predicted by the three finer solutions show convergence and at 10 diameters, our prediction of 10% is closer in line with 8 1/2% predicted by Benhamadouche et al. [5]. In addition, the average eddy viscosity in the sub-channel is showing the correct trend; as the mesh becomes finer less eddy viscosity is produced by the sub-grid model. These results seem to suggest that the present solutions are significantly under-resolved in the vicinity of the spacer grid strap trailing edge. They also suggest that the FE method is not overly dissipative. Higher resolution simulations of this geometry are planned for the future.

The next step in this study of the application of unstructured stabilized FE methods, to sub-assembly reactor core modeling, is to purse a detailed performance and parallel scaling study of this fully-implicit, fully-coupled NK solution method with AMG preconditioners. In addition, the code infrastructure supports higher order (*e.g.*, up to 8th order in space and 5th order in time) discretizations so that studies of the effectiveness of higher order approximations on resolution requirements, accuracy and time to solution for a given solution accuracy can also be carried out. A comparison of the current SUPG stabilized finite element discretization against a complete variation multiscale stabilization [20] is planned. Finally, alternate solution strategies that involve using a modified Newton method (freezing the Jacobian at each Newton step), a one-step Newton method and semi-implicit variants of time-stepping are all possible within the code's solver infrastructure and will be pursued. These modifications have the potential to significantly improve run time performance.

## 6. Acknowledgements

The authors would like to thank D. Z. Turner and S. B. Rodriguez for helpful discussions in carrying out the simulations. We also want to thank R. M. Garcia for his help with developing suitable meshing strategies for the 3x3 rod bundle geometry. Finally, we would like to thank Z. Karoutas and WEC for the 3x3 rod geometry file.

#### 7. References

- [1] Nicoud, F. and Ducros, F., "Subgrid-Scale Stress Modelling on the Square of the Velocity Gradient Tensor," Flow Turbulence and Combustion, Vol. 62, 1999, pp. 183—200.
- [2] Elmahdi, A.M., Lu, R., Conner, M.E., Karoutas, Z. and Baglietto, E., "Flow Induced Vibration Forces on a Fuel Rod by LES CFD Analysis," The 14th International Topical

- Meeting on Nuclear Reactor ThermalHydraulics, NURETH-14-365, Toronto, Ontario, Canada, Sept. 25-30, 2011.
- [3] Z. Karoutas, Jin Yan, M. Conner and A. Mandour, "Advanced Thermal Hydraulic Method Using 3x3 Pin Modeling," The 14th International Topical Meeting on Nuclear Reactor ThermalHydraulics, NURETH-14-338, Toronto, Ontario, Canada, Sept. 25-30, 2011.
- [4] CD-Adaptco, STAR-CCM, http://www.cd-adaptco.com/products/star\_ccm\_plus/index.xml.
- [5] Benhamadouche, S., Moussou, P. and Maitre, C. Le, "CFD Estimation of the Flow-Induced Vibrations of a Fuel Rod Downstream a Mixing Grid," Proceedings of the <u>ASME 2009</u> Pressure Vessels and Piping Division Conference, July 26-30, 2009, Prague, Czech Republic.
- [6] Abbasian, F., Yu, S.D. and Cao, J., "Large Eddy Simulation of Turbulent Axial Flow Along an Array of Rods," Journal of Fluids Engineering, vol. 132, 2010, pp. 1--11.
- [7] Smagorinsky, J., "General Circulation Experiments with the Primitive Equations," Monthly Weather Review, Vol. 3, 1963,pp. 99—164.
- [8] Kim, W.-W. and Menon, S., "A New Dynamic One-Equation Subgrid-Scale Model for Large-Eddy Simulation," AIAA Paper, AIAA-95-0356, 1995.
- [9] Fischer, P.F. and Iliescu, T., "A 3D Channel Flow Simulation at Re-tau=180 Using a Rational LES Model," 3<sup>rd</sup> AFOSR International Conference on Direct and Large Eddy Simulation TAICDL, 2001.
- [10] Hughes, T.J.R., "The Finite Element Method, Linear Static and Dynamic Finite Element Analysis, Dover, 2000.
- [11] Donea, J. and Huerta, A., "The Finite Element Method for Fluid Flow Problems", John Wiley and Sons, 2003.
- [12] Dennis, J.E.D. Jr. and Schnabel, R.B., "Numerical Methods for Unconstrained Optimization and Nonlinear Equations", SIAM, 1996.
- [13] J.N. Shadid, S.A. Hutchinson, G.L. Hennigan, H.K. Moffet, K.D. Devine and A.G. Salinger, "Efficient parallel computation of unstructured finite element reacting flow solutions," Parallel Computing, Vol. 23, 1997, pp. 1307 1325.
- [14] J.N. Shadid, R.S. Tuminaro, K.D. Devine, G.L. Henningan, P.T. Lin, "Performance of fully-coupled domain decomposition preconditioners for finite element transport/reaction simulations," J. Comput. Phys., Vol. 205, No. 1, 2005, pp. 24 47.
- [15] Saad, Y., "Iterative Methods for Sparse Linear Systems," SIAM, 2003.
- [16] P. T. Lin, M. Sala, J. N. Shadid and R. S. Tuminaro, "Performance of fully-coupled algebraic multilevel domain decomposition preconditioners for incompressible flow and transport," Int. J. Num. Meth. Eng, Vol. 67, 2006, pp. 208 225.
- [17] J.N. Shadid, A. G. Salinger, R. P. Pawlowski, P. T. Lin, G. L. Hennigan, R.S. Tuminaro and R. B. Lehoucq, "Large-scale Stabilized FE Computational Analysis of Nonlinear Steady State Transport / Reaction Systems," Comp. Meth. App. Mechanics and Eng., Vol. 195, 2006, pp. 1846 1871.
- [18] Turner, D. Z. and Rodriquez, S. B., Sandia National Laboratories, *Private Communication*, 2011.
- [19] CUBIT, http://cubit.sandia.gov/
- [20] T.J.R. Hughes, L. Mazzei, and K.E. Jansen, "Large Eddy Simulation and the variational multiscale method," Comp. Vis. Sci., Vol. 3, 2000, pp. 47 59.